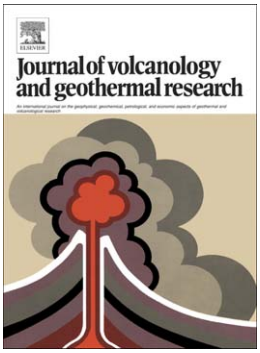

Preliminary report on the July 10–11, 2015 explosive eruption at Volcán de Colima: Pyroclastic density currents with exceptional runouts and volume.

L. Capra, J.L. Macías, A. Cortés, N. Dávila, R. Saucedo, S. Osorio-Ocampo, J.L. Arce, J.C. Gavilanes-Ruíz, P. Corona-Chávez, L. García-Sánchez, G. Sosa-Ceballos, R. Vázquez

PII: S0377-0273(15)00404-7
DOI: doi: 10.1016/j.jvolgeores.2015.11.022
Reference: VOLGEO 5716

To appear in: *Journal of Volcanology and Geothermal Research*

Received date: 24 August 2015
Accepted date: 23 November 2015

Please cite this article as: Capra, L., Macías, J.L., Cortés, A., Dávila, N., Saucedo, R., Osorio-Ocampo, S., Arce, J.L., Gavilanes-Ruíz, J.C., Corona-Chávez, P., García-Sánchez, L., Sosa-Ceballos, G., Vázquez, R., Preliminary report on the July 10–11, 2015 explosive eruption at Volcán de Colima: Pyroclastic density currents with exceptional runouts and volume., *Journal of Volcanology and Geothermal Research* (2015), doi: 10.1016/j.jvolgeores.2015.11.022

Preliminary report on the July 10-11, 2015 explosive eruption at Volcán de Colima: Pyroclastic density currents with exceptional runouts and volume.

Capra, L.[1], Macías, J.L.[2], Cortés, A.[3], Dávila, N.[4], Saucedo, R.[5], Osorio-Ocampo, S.[6], Arce, J.L.[7], Gavilanes-Ruíz, J.C.[8], Corona-Chávez, P.[7], García-Sánchez, L.[6], Sosa-Ceballos, G.[2], and Vázquez , R.[9]

[1]Centro de Geociencias, Universidad Nacional Autónoma de México, Juriquilla, Querétaro, México

[2]Instituto de Geofísica, Unidad Michoacán, Universidad Nacional Autónoma de México, Campus-Morelia, Morelia, 58090, Michoacán, México

[3]Centro Universitario de Estudios e Investigaciones de Vulcanología, Universidad de Colima, 28045, Colima, México

[4]Laboratorio de Sistemas de Información Geográfica, Facultad de Geografía, Universidad Autónoma del Estado de México

[5]Instituto de Geología, Universidad Nacional Autónoma de México, D.F., México

[6]Posgrado de Ciencias de la Tierra, Instituto de Geofísica, UNAM, México D.F.

[7]Instituto de Investigaciones en Ciencias de la Tierra, Universidad Michoacana de San Nicolás de Hidalgo, Morelia, 58040, Michoacán

[8]Licenciatura en Ciencia Ambiental y Gestión de Riesgos, Universidad de Colima, Colima 28045, México

[9]Posgrado de Ciencias de la Tierra, Centro de Geociencias, UNAM, México D.F.

November 11, 2015

Abstract

On July 10-11, 2015 an explosive eruption occurred at Colima volcano produced 10.5 km long pyroclastic density currents (PDCs) along the Montegrande, and 6.5 km long along the San Antonio ravines. The summit dome was destroyed and a new crater excavated and breached to the south. This new breach connects to a narrow channel that descends along Colima's southern flank and was used by a subsequent lava flow. The Montegrande PDCs represent the longest and hottest flow of this type recorded during the past 30 years but are still smaller in comparison to the 15-km long PDCs produced during the 1913 Plinian eruption. Data obtained from field reconnaissance, lahar monitoring stations, and satellite imagery suggest that at least six PDCs occurred. The two largest PDCs (H/L 0.2) were able to surmount topographic barriers or bends. Based on field reconnaissance and digital elevation models extracted from SPOT satellite imageries we estimate a minimum volume for the valley-pond and distal fan deposits of 4.5×10^6 m^3. After one week, the deposits were still hot with burning trees on the surface and millimeter-sized holes from which fumes were emanating. The juvenile components of the deposits consist of gray dense blocks and vesicular dark-gray blocks and bombs with bread-crust textures and cooling joints. The mineral association of these rocks consists of plagioclase + clinopyroxene + orthopyroxene + FeTi-oxides ± olivine and resorbed hornblende in a dark glassy matrix that corresponds to an andesitic composition.

1. Introduction and activity since November 2014

The Volcán de Colima, located in the western sector of the Trans-Mexican Volcanic Belt (Fig. 1) is the most active volcano in Mexico (Luhr, 1981; Medina, 1983; De la Cruz, 1993). The last major volcanic crises occurred in 2004-2005, and was characterized by several episodes of

dome growth and collapse accompanied by the emplacement of block-and-ash flows (BAFs) deposits that reached up to 7 km from the volcano's summit (Macías et al., 2006; Sulpizio et al., 2010). In 2007, a new summit dome growth slowly until June 2011. Afterwards, the volcano did not show any important activity until early 2013. On January 6, 2013 a new vulcanian explosive phase culminated on January 29 with the destruction of the 2007-2011 lava dome (Zobin et al., 2015). The excavated crater was then filled by a new dome. In March 2013 the lava overspilled the crater rim, and descended towards the west advancing a few hundred meters (GVP, 2013). From this time and until July 2014 only small explosions and rock falls were detected at the volcano (Zobin et al., 2015). In September 2014, renewed effusive activity formed a new dome and the emplacement of a lava flow on the SW slope of the volcano that advanced 1.5 km from the summit. On November 21 an ash plume rose ~7 km above the crater from which a 3-km long PDC descended along the San Antonio ravine (GVP, 2014). In January 2015 several explosions caused the partial destruction of the dome and generated a 3-km ash plume that dispersed ash toward the NE (GVP, 2015a). Afterwards, two lava flows were active on the W-SW flanks showing a minimal advance (GVP, 2015b). In February 2015, the volcano produced several gas-and-ash plumes per day rising to altitudes of 5.5-7.3 km (GVP, 2015c). Similar activity continued through the following months. In May, a thermal anomaly was detected inside the crater suggesting a new dome extrusion phase (GVP, 2015d) that by the beginning of June was overflowing the SW rim of the crater. In early July two main lava flows were rapidly advancing (few hundred meters), one on the northern flank, and the largest one on the southern slope. During July 7-9 a gradual increase in the frequency of ash plumes, rock falls,

and small PDCs was observed (GVP, 2015e), and by July 10 a lava flow had reached ~700 m down the southern flank (Fig. 2a).

2. The July 10-11, 2015 event

On July 10, at 12 hrs (all times are given in local time and over 24 hrs) an ash plume rose up to 7.7 km a.s.l. and drifted 150 km to the west. At 20:17 hrs the paroxysmal activity began, with the formation of PDCs that descended on the southern slope and became channeled into the Montegrande ravine (Fig. 2b). Coevally, a 4-km high ash plume associated to the ash clouds accompanying the PDCs drifted towards the west blanketing with ash the communities of La Yerbabuena (5-cm-thick layer), La Becerrera, San Antonio, Carrizalillo, El Naranjal, Nuevo Naranjal, and Suchitlán (18 km SSW) (Fig. 1b). Few hours later, the Unidad Estatal de Protección Civil de Colima promoted and assisted the voluntary evacuation of residents of La Yerbabuena and other nearby villages totaling 70 people (GVP, 2015f). On July 11, at 13:50 hrs, PDCs flowed through the Montegrande ravine into a flat volcaniclastic plain and nearly reached high-tension electric power lines as witnessed by José Velázquez worker of the the Comisión Federal de Electricidad (CFE). These PDCs seem to be those reported by the GVP to have occurred on July 11 (GVP, 2015f) that reached a maximum distance of 10.5 km (Fig. 2b).

Since 2011, systematic lahar monitoring has been carried out at the Montegrande and since 2013 at La Lumbre ravines (Fig. 1b) by one of the authors (L. Capra) in collaboration with the RESCO seismological network of Universidad de Colima and the Centro Nacional de Prevención de Desastres (CENAPRED). Each monitoring site was equipped with several sensors including a video camera that recorded the initial eruptive phase on July 10 (Fig. 3). The camera located at

6.5 km from the volcano's summit in the Montegrande ravine was able to record initial PDCs. At 20:31 hrs, a first PDC that stopped ~300 m upstream from the monitoring site was detected. At 20:33 hrs, the main front of a second PDC pulse was recorded (Fig. 3a) and at 20:34 hrs a dilute PDC overrun the camera, and communication was lost because the monitoring equipment was destroyed (Fig. 4). Around the same time (20:32 hrs), the camera installed at the La Lumbre monitoring site recorded ash fall, which continued for several minutes until the communication was also interrupted (Fig. 3b). At this site, 2 cm of ash blanketed the instrumentation. After the emplacement of the PDCs, a lava flow started to flow down from the new crater (Fig. 5).

3. Morphology of the summit crater and post-eruptive activity

After the July 10-11 activity, the morphology of the summit area displayed important changes (Figs. 5a and b). The summit dome was destroyed and a new crater was excavated. The most striking feature of the crater was a ~130-m wide breach open to the SE (Fig. 5b). Such a morphological change had never been observed during the modern activity of Colima. After the explosive phase, a lava flow began to descend through the breach and into the ~100- m wide and several meters-deep channel (Fig. 5b and c). This new depression was likely produced prior to or during the occurrence of the largest PDCs recorded on July 10 or 11.

During fieldwork performed in July 2015, Volcán de Colima was constantly emitting a gas column that rose several kilometers above the crater. In August, the volcano was very active producing vulcanian-type explosions that generated dark-gray ash plumes that rose 2-3 km above the crater. Few stronger explosions launched ballistics on the cone's flanks and dispersed ash that fell up to 7 km from the volcano.

The lava flow that between July 15 and 17 had descended more than half of the distance between the crater breach and the break in slope, had reached 2.1 km from the summit on July 23 (Fig. 5c), and 2.5 km on August 6, when it divided in two lobes (Fig. 5c). Blocks from the unstable lava flow front were continuously collapsing producing small PDCs.

4. The deposits

Between July 10 and 11 several PDCs were channeled either into the Montegrande or into the San Antonio ravines reaching 10.5 and 6.5 km from the crater, respectively (Fig. 2b). The PDCs along the Montegrande ravine followed the main channel that narrows or widens in some parts prior to debouching into a flat open plain where electric power lines cross the ravine. These PDCs filled the ravine and stopped at about 5 km upstream from the village of Quesería inhabited by 8,611 people (INEGI, 2010). The deposits are gray in color and have lobated fronts and well-developed lateral levees. The deposits belong to a valley-pond facies within the ravine (block-and-ash flow deposits, BAFs) or to an overbank facies where they occur as massive (BAFs) or dune bedded with internal cross-stratification dilute PDC deposits.

Before the July 10-11 eruption, the Montegrande ravine was an active channel continuously eroded by lahars triggered each year during the rainy season (Capra et al., 2010; Vázquez et al., 2014). The active channel was up to 3-4 m wide and bounded by several lahar terraces (1-6 m high) formed in previous years (Figs. 4a-b). These terraces were delimited by the 20-25-m high ravine walls made by the 1818 and 1913 Plinian pyroclastic deposits (Saucedo et al., 2010), debris avalanche deposits associated to the failure of previous edifices that occurred during the

Holocene and late Pleistocene (Cortés et al., 2005; Roverato et al., 2011), and fallouts of past Colima eruptions.

The Montegrande monitoring station was built on a 13 m high terrace, and the active channel where previous lahars were detected was up to 3 m in width (Figs. 4a and b). The monitoring system consisted of a 15 m high tower buried in concrete for 1.5 m, supporting 4 solar panels, 4 power batteries (200 kg in total weight) and a camera (Figs. 4b). As mentioned above the instrumentation was completely swapped away by the July 10 PDCs (Figs. 4c-d). In fact, the terrace where the tower was settled was covered by a 2-m thick massive overbank deposit (BAF) and mantled on top by a 2 cm ash deposit. By considering the previous morphology of the ravine at this site, the approximate thickness of the ponded BAF deposits in the middle of the channel is ca. 8- m. On the valley sides the overbank deposits are up to 2 m in thickness (Figure 6a) and lateral walls of the ravine show meter-size striations (Fig. 6b). At 1.8 km up valley from the monitoring site, the Montegrande ravine is separated by a 200 m-wide relieve from the San Antonio ravine (Figs. 1b and 7a). At this point the PDCs were able to overrun this relieve and partially flow into the San Antonio ravine (Fig. 7b-c) where they emplaced ca. 3 m thick deposits. Based on the topographic profile (Fig. 7d) and field evidence the valley-pond BAF deposits in the middle of the Montegrande ravine channel are up to 20 m in thickness. Here, the dilute PDCs were able to overrun a 15 m high topographic obstacle. 800 m upslope from this point, the Montegrande ravine was interrupted by a 15 m-thick lava flow wall where “cascading lahars” (Fig. 3b in Capra et al., 2010) have been observed during the rainy season (Fig. 8a). Now, only 1.2 m of the upper part of the lava flow wall crops out (Fig. 8b) indicating that the ponded BAF deposits are ~14 m thick. Here, the deposit surface consists of at least two

lateral, block-rich levees (Fig. 8c) and lahar deposits are already observable filling these channels. In fact, few days after the eruption, rainfall was recorded at the volcano, triggering these lahars. At this location a lahar had been emplaced the day before our visit and was still at 56°C. From this point we walked up to the lava flow front that on August 6 has reached 2.5 km from the crater (Figs. 5c and 9b). At the same distance, on a lateral terrace, a metallic box was installed in 2009 to sample fine ash emplaced by dilute PDCs (Figs. 9a-c). The box was approximately 80 kg in weight, sustained by a 4 cm in-diameter steel rod buried in concrete, and the four corners of the box were fixed with steel wires (Fig. 9c). The metallic box resisted the July dilute PDCs, in fact, the steel rod was just bent and it had cm-size impact prints on its frontal side (Fig. 9d). Trees were partially burned and blown down on the hill where the box was settled (Fig. 9e). The box was filled with fine ash, the same material was exposed on top of this terrace where several ash layers were recognized (Fig. 9e). At the top of a contiguous hill, we identified at least six different dune-bedded with internal cross stratification dilute PDC deposits separated by erosive contacts on top of a white discontinuous ash fall layer with charbonized leaves. We interpret the cross-bedded layers as the dilute counterparts of six different dense PDCs.

The distal tip of the BAF deposits corresponds to the main fan where lahars usually pile up (Figs. 2b and 10a). In this volcaniclastic fan area two main lobes of the BAF deposits are observable, and their surface consists of lava blocks up to 2 m in diameter surrounded by a lapilli-to-ash matrix. No pumice fragments were recognized among the juvenile components. Juvenile fragments are dark-gray in color and commonly show cooling fractures or bread-crust surfaces, and many of them are scoriaceous and vesicular (Fig. 10b). Hand specimens of these juvenile

blocks show in order of decreasing abundance plagioclase + clinopyroxene + orthopyroxene + Fe-Ti oxides ± olivine and glomerocrysts. Juvenile samples collected at the monitoring station and from the lava flow front include the same paragenesis plus anomalously large crystals of hornblende that are larger than any of the other mineral phases. They show resorbed margins suggesting a xenocrystic origin. Large blocks of lava show impact marks, but few of them also show striations with glassy surfaces (Fig. 10c). Sporadically, on the surface of the deposits occur 2-3 m wide and ~0.6 m-deep "ash pools". These depressions consist of very fine ash that in August 6 was water saturated because of the rainfalls (Fig. 10d). Shortly before the Montegrande ravine exits into the volcaniclastic fan, the PDCs were still able to overrun 8 to 10 m high topographic barriers (Fig. 11a-b). The dilute PDCs draped the upper portions of the ravine channel partially bending and burning trees and leaving up to 12 cm of fine ash (Fig. 11 c-d).

5. Volume estimation

The volume of the valley-pond and of the distal fan deposits was calculated based on digital surface models (DSMs) extracted from SPOT stereopares images, one acquired on November 21, 2014 (before the eruption) and another on July 25, 2015 (after the eruption, Fig. 2b). The DSM was obtained by photogrammetry (angular distance) using ground control points (GCPs) from INEGI orthophotos at 1:10,000 scale. The final horizontal resolution of both DSMs was 21 m. The cut-and-fill function available in ©ArcMap 10.2 was used to calculate the volume. Figure 12a shows the result with a net gain value of 4.5 $X10^6$ m^3 which could be considered as the average value of the volume for the valley-pond and distal fan deposits along Montegrande

ravine. The calculation also gives an apparent lost of volume, in particular where the PDCs were able to flow into the San Antonio ravine, and where the channel narrows. The DSMs here obtained represent the model of the surface which include vegetation, so the lost in volume could either reflect the area where vegetation was blown down, such as at the junction of the San Antonio ravine (Fig. 7 and profile I in Fig. 12a) or the uncertainty between the DSM's accuracies in the photogrammetry processes in the narrowest portion of the valley (profile II, Fig. 12a). The volume of the deposit here estimated is at least four times larger than those estimated for previous PDCs at Volcán de Colima that have occurred during the last 25 years (Rodríguez-Elizarrarás et al., 1991; Saucedo et al., 2002; Saucedo et al., 2004; Macías et al., 2006; Sulpizio et al., 2010).

The DSM of the deposits was also obtained by a simple raster operation (subtraction) between the pre and post eruption DSMs. The deposit's isopachs were then extracted from the DSM, showing maximum thicknesses of 20 m in the valley-pond area (Fig. 12b), and of 6-8 m in the distal reach (Fig. 12c). These values correspond with field observations as described before.

6 Discussion and conclusions

Since the 1913 Plinian eruption, the largest activity recorded in the modern eruptive record (VEI = 4, Saucedo et al., 2010), the July 10-11 eruption generated by far the largest PDCs produced by the volcano. The 1913 eruption destroyed the summit dome excavating 400 m of the summit crater and producing 15 km-long PDCs and a Plinian fallout that was dispersed to the NE (Saucedo et al., 2010; Bonasia et al., 2011). In 1962, 49 years after the 1913 eruption, the Colima's crater was filled again and the formation of summit domes, lava flows, and PDCs

initiated (Bretón et al., 2002; Saucedo et al., 2005; Saucedo et al., 2010). Since then, Volcán de Colima has slowly increased its activity with stronger explosions and PDCs with longer run outs. Indeed, PDCs have increased in volume with time (up to $1*10^6$ m^3) and their runouts from 5.5 km in 1991, 6.5 km in 1998-2002, to 6.5 km in 2004-2005 which correspond to H/L ratios ranging from 0.47 to 0.28 (Saucedo et al., 2004; Sulpizio et al., 2010). Until 2005, all PDCs were either produced by lateral collapse of the summit dome (e.g. Merapi-type events, Rodríguez-Elizarrarás, 1991) or by the partial destruction of the summit dome accompanied by explosions (e.g. Soufriere-type events, Saucedo et al., 2002; Macías et al., 2006; Sulpizio et al., 2010). These PDCs usually have emplaced massive, valley-pond deposits and overbank stratified PDC deposits. The July 10-11 activity completely destroyed the summit dome, breached part of the crater, and produced a significant erosion channel on the upper cone (Figs. 5b an c). The H/L ratio estimated for the largest Montegrande PDCs described in this study is 0.2 and by far the lowest ever recorded in recent decades.

The July 10-11 activity sheds new light on the eruptive behavior of Volcán de Colima for two main reasons. First, it produced PDCs with the longest runout since the 1913 eruption, reaching 10.5 km from the summit, and second, part of the juvenile components contained within the deposits are scoriaceous and vesicular, suggesting that internal parts of the summit dome were hotter, rich in gas, under pressure and involved in triggering the collapse. This information suggests that the continuous ascent of andesitic magma to the surface produced the instability of the growing dome and the generation of rocks falls, and small PDCs recorded in early July (GCP, 2015e). As magma ascent continued, the southern upper part of the cone failed breaching the summit crater and eroding a narrow channel down to the base of the cone (Fig.

5). Breaching and collapse of this part of the cone was immediately followed by the collapse of the summit dome generating a series of PDCs on July 10. The largest PDCs destroyed the lahar monitoring station at the Montegrande ravine and were able to reach the volcaniclastic fan. The activity continued until July 11 when another set of PDCs with similar runouts occurred. The eruption ended with the emplacement of a lava flow representing the volume of the degassed magma left in the conduit. The gas-rich portions of the collapsing dome were easily fragmented during transport increasing progressively the content of gas and fine ash in the moving PDCs. Therefore, besides the PDC's volume, internal gas-rich parts of the dome (scoriaceous and vesicular fragments), and fine ash probably favored the mobility of the PDCs by promoting an increase in the gas pore-pressure in the mixture. Nevertheless, vertical exposures of the deposits are not available yet to accomplish a detailed textural and granulometric study to constrain the mechanism of emplacement. The large ash clouds observed in the southwestern sector of the volcano since the beginning of the activity and the "ash pools" on the distal portion of the deposits (Fig. 10d) are evidence of larger volumes of gas and ash involved in the PDC's mixture. The "ash pools" can be interpreted as post-depositional degassing sites, probably in correspondence of concentration of buried large juvenile fragments. No explosive activity was recognized contemporaneously to the eruption, so fragmentation only occurred during the initial dome failure and during the PDCs transport.

This extraordinary eruption highlights the need to revise the hazard assessment for this type of scenario, as PDCs from dome collapse with such great mobility were not previously considered (Saucedo et al., 2005; Sulpizio et al., 2010; Capra et al., 2015).

Acknowledgments

The SPOT images where obtained through a collaborative agreement between the Universidad Autónoma del Estado de México and the Agrifood-Fishery Mexican Service (SIAP) - ERMEX, under the license of "Airbus Defense & Space". LANDSAT images are a courtesy of the U.S. Geological Survey by the Global Visualization Viewer (GLOVIS) program. This work was partially supported by CONACyT 220786 project granted to Lucia Capra. The Montegrande and La Lumbre monitoring sites are operated by L. Capra in collaboration with G. Reyes at the RESCO seismological network of Universidad de Colima and the Centro Nacional de Prevención de Desastres (CENAPRED). The manuscript benefits from the constructive reviews of C. Siebe and R. Sulpizio.

Figure Captions

Figure 1. a) Sketch map of the Trans Mexican Volcanic Belt (TMVB) showing the location of Volcán de Colima (VC). Black triangles represent main active volcanoes in Mexico. b) SPOT satellite image acquired on April 7, 2015, showing the locations of the two monitoring sites where videocameras captured the front of the first PDCs (Montegrande MS), and the ash fall (La Lumbre MS).

Figure 2. a) Operational Land Imager (OLI) Landsat Image (bands 6, 5 and 4 in red-green-blue colors, 15 m in resolution) acquired on July 10, 2015 just prior to the eruption (Courtesy of U.S. Geological Survey by Global Visualization Viewer (GLOVIS)). The lava flow is clearly visible, extending up to ~700 m towards the Montegrande ravine, incandescent material is observable up to 2.5 km from the crater. b) SPOT image acquired on July 25, 2015 (2.5 m in resolution) obtained with a fusion process between a multispectral image of 10 m in resolution and panchromatic data. This image shows the distribution of the PDCs along the Montegrande

ravine, up to the distal fan. The Montegrande monitoring site and the location of the steel box for ash sampling are also indicated.

Figure 3. Recorded images from the Montegrande and La Lumbre monitoring sites. a) The first PDC front caught by the camera at 20:31 hrs, after that moment the system stopped transmitting data. b) Three minutes after the detection of the PDC front, the camera at the La Lumbre monitoring site recorded ash fall.

Figure 4. Pictures of the Montegrande MS (M-MS) before and after the emplacement of PDCs (see Fig. 2 for location). a) Zoom of the April 7, 2015 SPOT image indicating the location of the monitoring site and b) picture taken on June 2015. The black arrow points at the 15-m high tower (inset). b) Zoom of the July 25, 2015 SPOT image indicating the location of the M-MS after the event and d) panoramic view of the M-MS (white arrow) taken on August 6, 2015.

Figure 5. a) Panoramic view of Volcán de Colima taken in 2013 from the point where the still box was installed (see Fig. 2 for location). b) View of the volcano taken on August 6, 2015 from the same location, the black arrow points at the new lava flow. The inset shows the scarp formed on the summit after the dome collapse. c) EO-1 ALI image (NASA's New Millennium Program-NMP) acquired on July 23, 2015 . Its resolution was improved by a fusion process between a multispectral image (30 m) and panchromatic data (10 m) (4, 3 and 2 bands in red-green-blue colors). The new lava flow emplaced after the dome collapse episode is clearly visible. The yellow dot corresponds to the maximum extent of the lava flow (LF) as observed on August 6. The inset shows a zoom on the crater where the scarp formed by the dome collapse is visible.

Figure 6. a) View of the channel at the Montegrande MS showing a 2 m-thick overbank BAF deposit covered by 2 cm of massive ash. b) Picture taken a few hundred meters upstream from the Montegrande MS showing flow scratches on lateral terraces (white arrows).

Figure 7. Images showing morphological changes at the junction between the San Antonio and Montegrande ravines (see Fig. 2 for location). Zoom of a) April 7 and b) July 25, 2015 SPOT images displaying PDCs that were able to surmount the topographic high that subdivides the two ravines. c) Picture of the San Antonio ravine taken from this site. d) Topographic profile at the point where the PDCs were able to overtop towards the San Antonio ravine.

Figure 8. Photos of the Montegrande ravine in its proximal reach (see Fig. 2 for location). a) View of a 15 m-thick lava flow where usually "lahar cascade" formed during the rainy season, and b) picture of the same site, where the lava flow is partly buried by a ponded facies of the PDCs. c) Above the lava obstruction at least two lateral levees left by PDCs are observable (white arrows) now serving as channel sides for the first lahars recorded (brown area).

Figure 9. Images showing the effects of PDCs caused in the proximal reaches where a steel box for ash sampling was installed in 2009 (see Fig. 2 for location). a) and b) show SPOT images before and after the eruption showing the location of the steel box (white circle). Pictures of the box before (c) and after the eruption (d). e) Cm-sized impact marks observed on the frontal side of the box. f) View of the hill where the box was installed, vegetation was partially burned and bent, and the dilute PDCs emplaced massive and stratified fine ash layers (inset).

Figure 10. a) View of the distal fan where the PDCs stopped. Meter-sized lava blocks are observable on the surface. b) Some juvenile fragments are banded showing different degrees of vesiculation. C) On the surface of the largest lava blocks impact features are common (white circle) and few glassy striations are also observable (white arrow). d) On the surface of the deposit "ash pools" filling sagging areas are very common, easily recognizable after the first rains.

Figure 11. Satellite images of the distal area before (a) and after (b) the eruption. The white arrow points to the location where the PDCs were able to overflow a topographic barrier reached the fan. c) Photo showing the Montegrande ravine just before the distal fan. Here it is

possible to observe how the PDCs overrun lateral terraces, burning vegetation and leaving massive deposits (d). The vegetation below the fine ash is not burnt.

Figure 12. a) Raster map obtained by applying the cut-and-fill function (©ArcMap 10.2) using the November 21, 2014 and the July 25, 2015 DSMs. The net gain ($4.5x10^6$ m^3) corresponds with the volume estimated for the valley-pond and distal fan of the PDC deposits. Topographic profiles show deposit's thickness. Based on the DSM of the deposit, isopach maps where generated for the proximal (b) and distal (c) reaches of the deposit.

References

Bonasia, R., Capra, L., Costa, A., Macedonio, G., Saucedo, R., 2011. Tephra fallout hazard assessment for a Plinian eruption scenario at Volcán de Colima (Mexico). Journal of Volcanology and Geothermal Research 203, 12-22.

Bretón, M., Ramírez, J.J., Navarro, C., 2002. Summary of the historical eruptive activity of Volcán de Colima, México: 1519-2000. Journal of Volcanology and Geothermal Research 117, 21–46.

Capra, L., Gavilanes-Ruiz, J.C., Bonasia, R., Saucedo, R., Sulpizio, R., 2015. Re-assessing volcanic hazard zonation of Volcán de Colima, México. Natural Hazards 76, 41-61.

Capra, L., Borselli, L., Varley, N., Norini, G., Gavilanes, J. C., Sarocchi, D., Caballero, C., 2010. Rainfall-triggered lahars at Volcán de Colima, Mexico: surface hydro-repellency as initiation process. Journal of Volcanology and Geothermal Research 189(1-2), 105-117.

Cortés, A., Garduño-Monroy, V.H., Navarro-Ochoa, C., Komorowski, J.C., Saucedo, R., Macías, J.L., Gavilanes, J.C., 2005. Cartas Geológicas y Mineras 10. Carta Geológica del Complejo Volcánico de Colima, con Geología del Complejo Volcánico de Colima: México D.F., Universidad Nacional Autónoma de México, Instituto de Geología, escala 1:10,000, mapa con texto explicativo 37 p., 15 figs., 2 tablas.

De la Cruz-Reyna, S., 1993. Random patterns of occurrence of explosive eruptions at Colima Volcano, Mexico. Journal of Volcanology and Geothermal Research 55 (1), 51-68.

GVP, 2013. Report on Colima (Mexico). In: Wunderman, R. (Ed.), Bulletin of the Global Volcanism Network, 38: 4. Smithsonian Institution

GVP, 2014. Report on Colima (Mexico). In: Sennert, S.K. (Ed.), Weekly Volcanic Activity Report, 19 November-25 November 2014. Smithsonian Institution and US Geological Survey.

GVP, 2015a. Report on Colima (Mexico). In: Sennert, S .. (Ed.), Weekly Volcanic Activity Report, 7 January-13 January 2015. Smithsonian Institution and US Geological Survey.

GVP, 2015b. Report on Colima (Mexico). In: Sennert, S.K. (Ed.), Weekly Volcanic Activity Report, 28 January-3 February 2015. Smithsonian Institution and US Geological Survey.

GVP, 2015c. Report on Colima (Mexico). In: Sennert, S.K. (Ed.), Weekly Volcanic Activity Report, 18 February-24 February 2015. Smithsonian Institution and US Geological Survey

GVP, 2015d. Report on Colima (Mexico). In: Sennert, S.K. (Ed.), Weekly Volcanic Activity Report, 13 May-19 May 2015. Smithsonian Institution and US Geological Survey.

GVP, 2015e. Report on Colima (Mexico). In: Sennert, S.K. (Ed.), Weekly Volcanic Activity Report, 8 July-14 July 2015. Smithsonian Institution and US Geological Survey.

GVP, 2015f. Report on Colima (Mexico). In: Sennert, S.K. (Ed.), Weekly Volcanic Activity Report, 8 July-14 July 2015. Smithsonian Institution and US Geological Survey.

Instituto Nacional de Estadística y Geografía (INEGI), 2010. Censo de Población y Vivienda. Estado de Colima. http://www.censo2010.org.mx/

Luhr, J.F., 1981. Colima: History and cyclicity of eruptions. Volcano News 7, 1-3.

Macías, J.L., Saucedo, R., Gavilanes, J.C., Varley, N., Velasco García, S., Bursik, M. I., Vargas Gutiérrez, V., Cortes, A., 2006. Flujos piroclásticos asociados a la actividad explosiva del volcán de Colima y perspectivas futuras. GEOS 25 (3), 340-351.

Medina, F., 1983. Analysis of the eruptive history of the Volcán Colima, México (1560-1980). Geofis. Int. 22, 157-178.

Rodríguez-Elizarrarás, S., Siebe, C., Komorowski, J.C., Espíndola, J.M., Saucedo, R., 1991. Field observations of pristine block-and ash-flow deposits emplaced April 16–17, 1991 at Volcan de Colima, Mexico. Journal of Volcanology and Geothermal Research 48 (3), 399-412.

Roverato, M., Capra, L., Sulpizio, R., Norini, G., 2011. Stratigraphic reconstruction of two debris avalanche deposits at Colima Volcano (Mexico): Insights into pre-failure conditions and climate influence. Journal of Volcanology and Geothermal Research 207, 33-46.

Saucedo, R., Macías, J.L., Gavilanes, J.C., Arce, J.L., Komorowski, J.C., Gardner, J.E., Valdez, G., 2010. Eyewitness, stratigraphy, chemistry, and eruptive dynamics of the 1913 Plinian eruption of Volcan de Colima, Mexico. Journal of Volcanology and Geothermal Research 191, 149-166.

Saucedo, R., Macías, J.L., Sheridan, M.F., Bursik, M.I., Komorowski, J. C., 2005. Modeling of pyroclastic flows of Colima Volcano, Mexico: implications for hazard assessment. Journal of Volcanology and Geothermal Research 139 (1), 103-115.

Saucedo, R., Macías, J.L., Bursik, M.I., 2004. Pyroclastic flow deposits of the 1991 eruption of Volcán de Colima, Mexico. Bulletin of Volcanology 66, 291-306.

Saucedo, R., Macías, J.L., Bursik, M. I., Mora, J.C., Gavilanes, J.C., Cortes, A., 2002. Emplacement of pyroclastic flows during the 1998-1999 eruption of Volcan de Colima, Mexico. Journal of Volcanology and Geothermal Research 117 (1-2), 129-153.

Sulpizio, R., Capra, L., Sarocchi, D., Saucedo, R., Gavilanes, J.C., Varley, N., 2010. Predicting the block-and-ash flow inundation areas at Volcán de Colima (Colima, Mexico) based on the present day (February 2010) status. Journal of Volcanology and Geothermal Research 193, 49-66.

Vázquez, R., Capra, L., Caballero, L., Arámbula-Mendoza, R., Reyes-Dávila, G., 2014. The anatomy of a lahar: Deciphering the 15 th September 2012 lahar at Volcán de Colima, Mexico. Journal of Volcanology and Geothermal Research 272, 126-136.

Zobin, V.M., Arambula-Mendoza, R., Breton, M., Reyes, G., Placencia, I., Navarro, C., Téllez, A., Campos, A., González, M., León, Z., Martínez, A., Ramírez, C., 2015. Dynamics of the January 2013–June 2014 explosive-effusive episode in the eruption of Volcán de Colima, México: insights from seismic and video monitoring. Bulletin of Volcanology and Geothermal Research 77, 31-44.

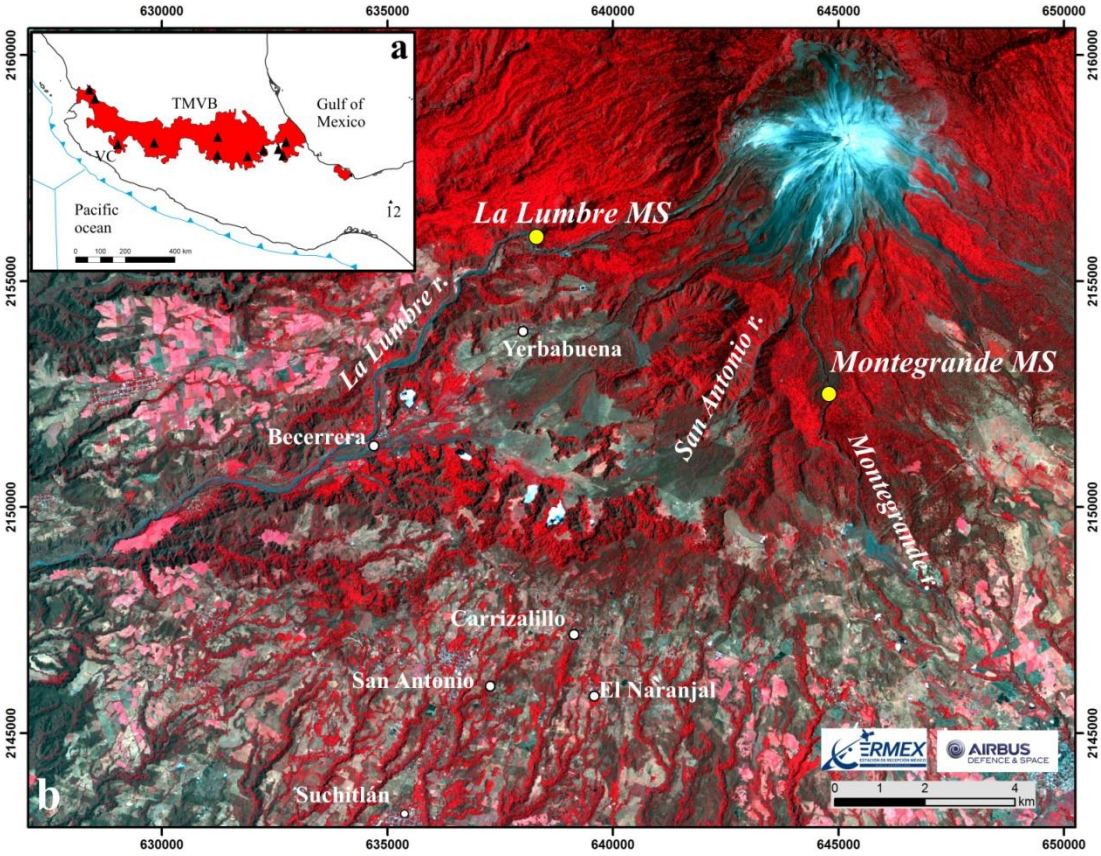

Figure 1

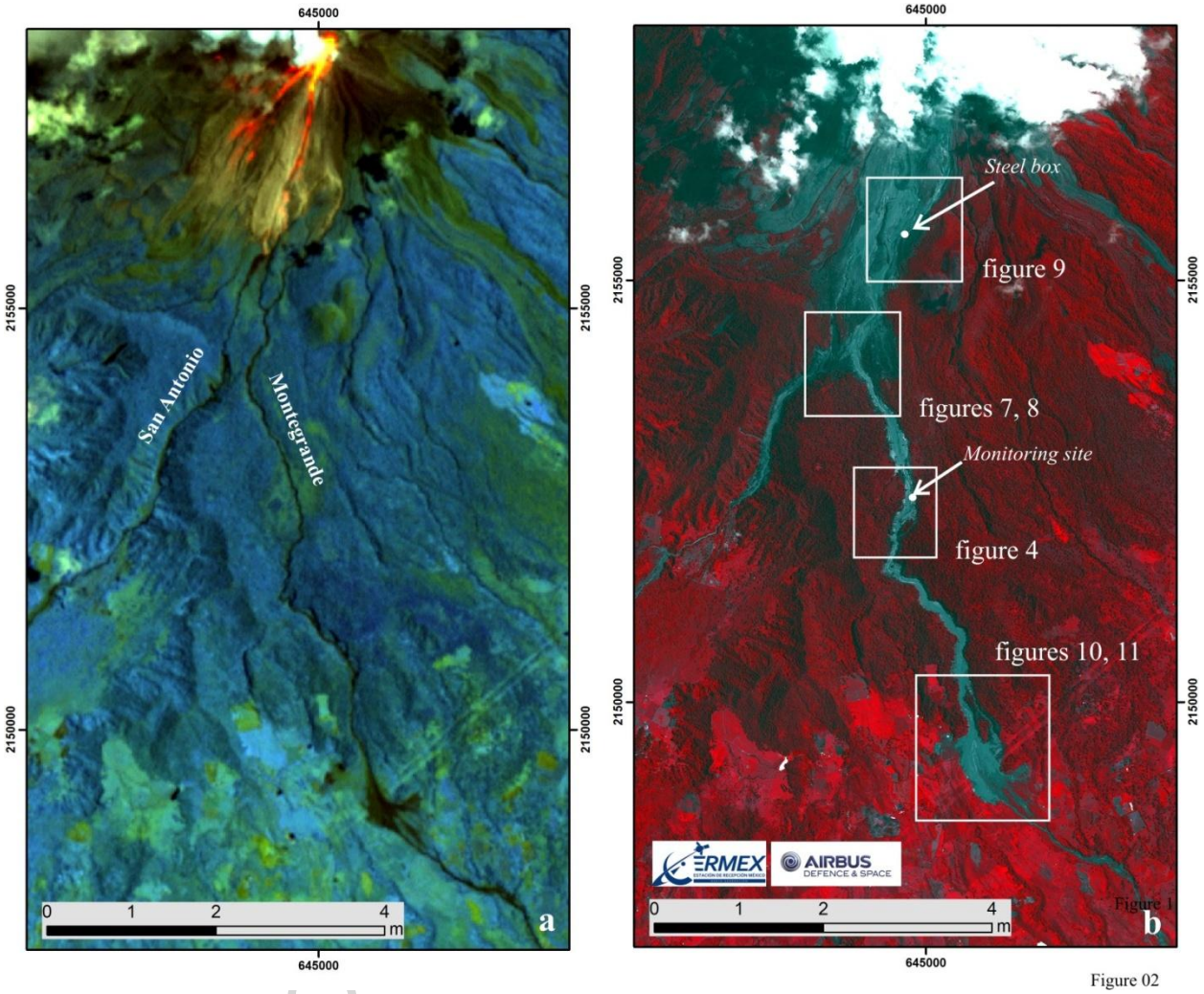

Figure 02

Montegrande MS

La Lumbre MS, 3 minutes after

Figure 3

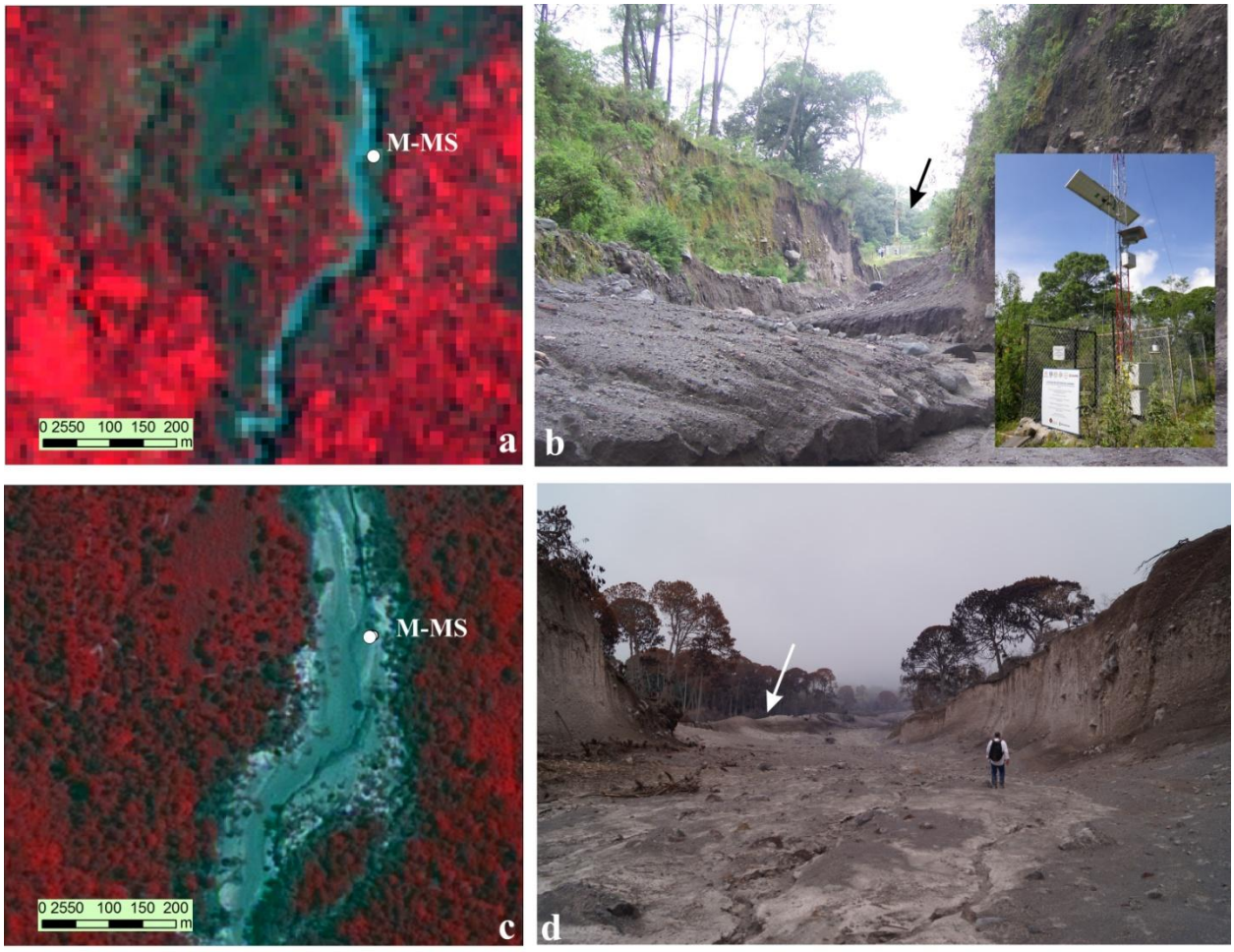

Figure 4

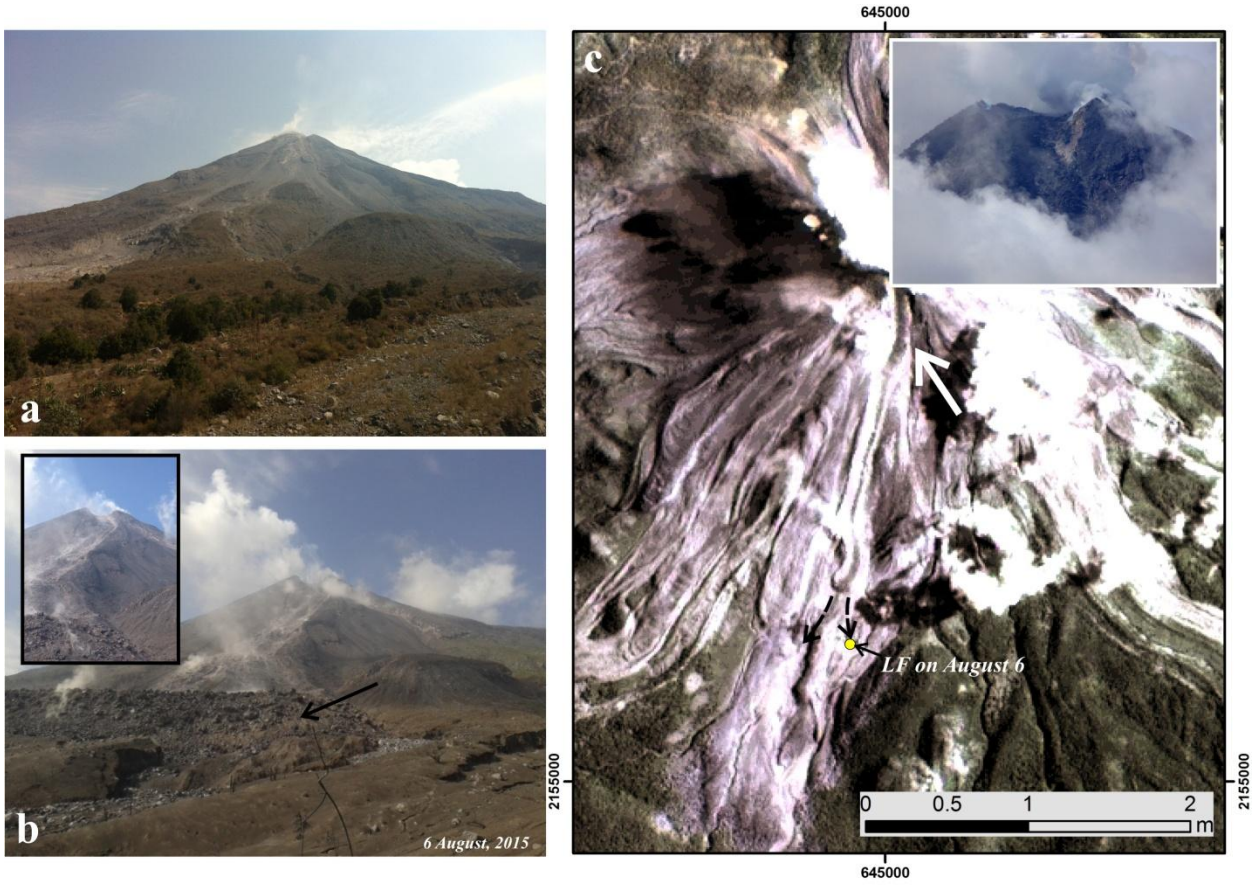

Figure 05

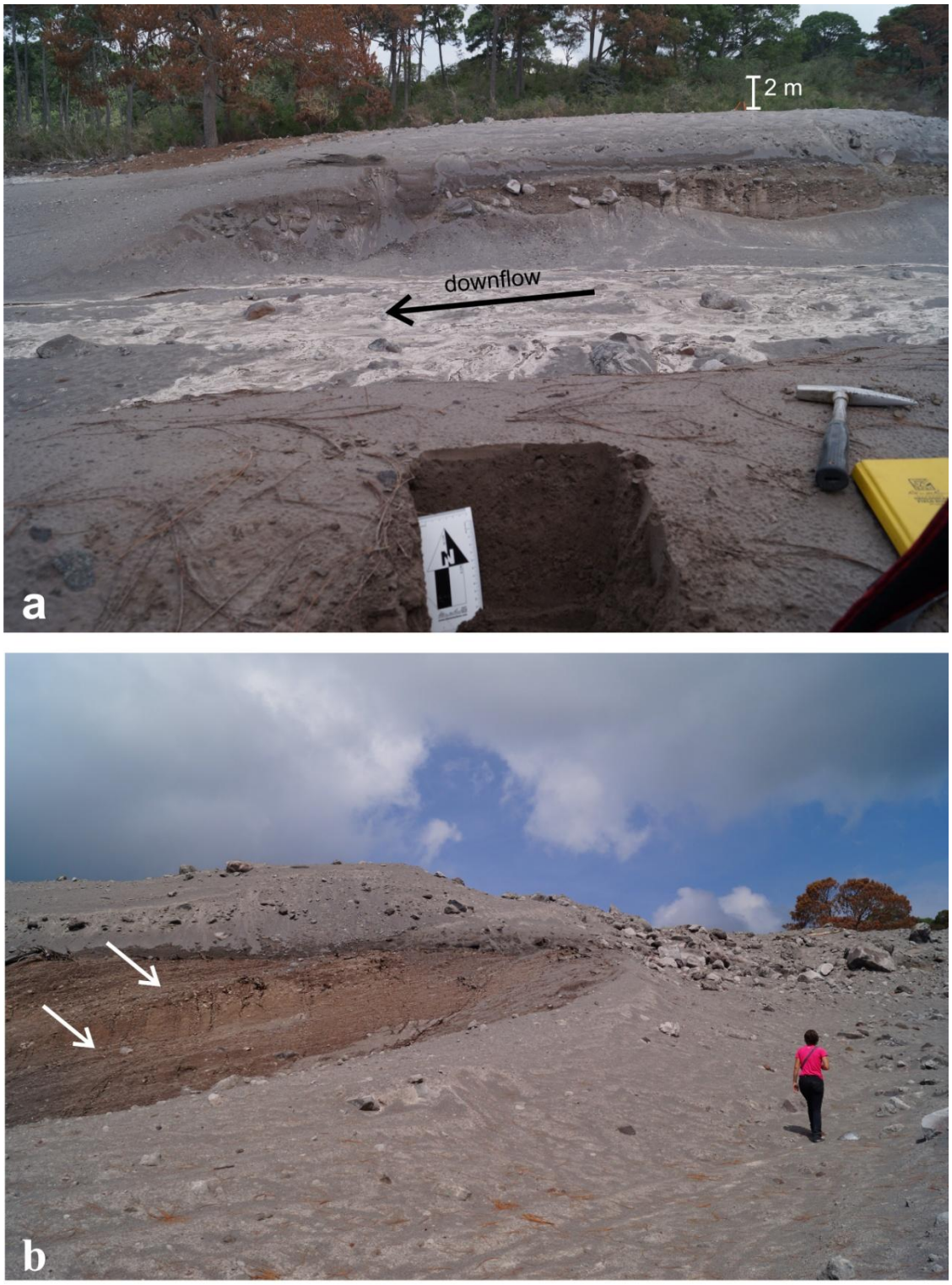

Figure 06

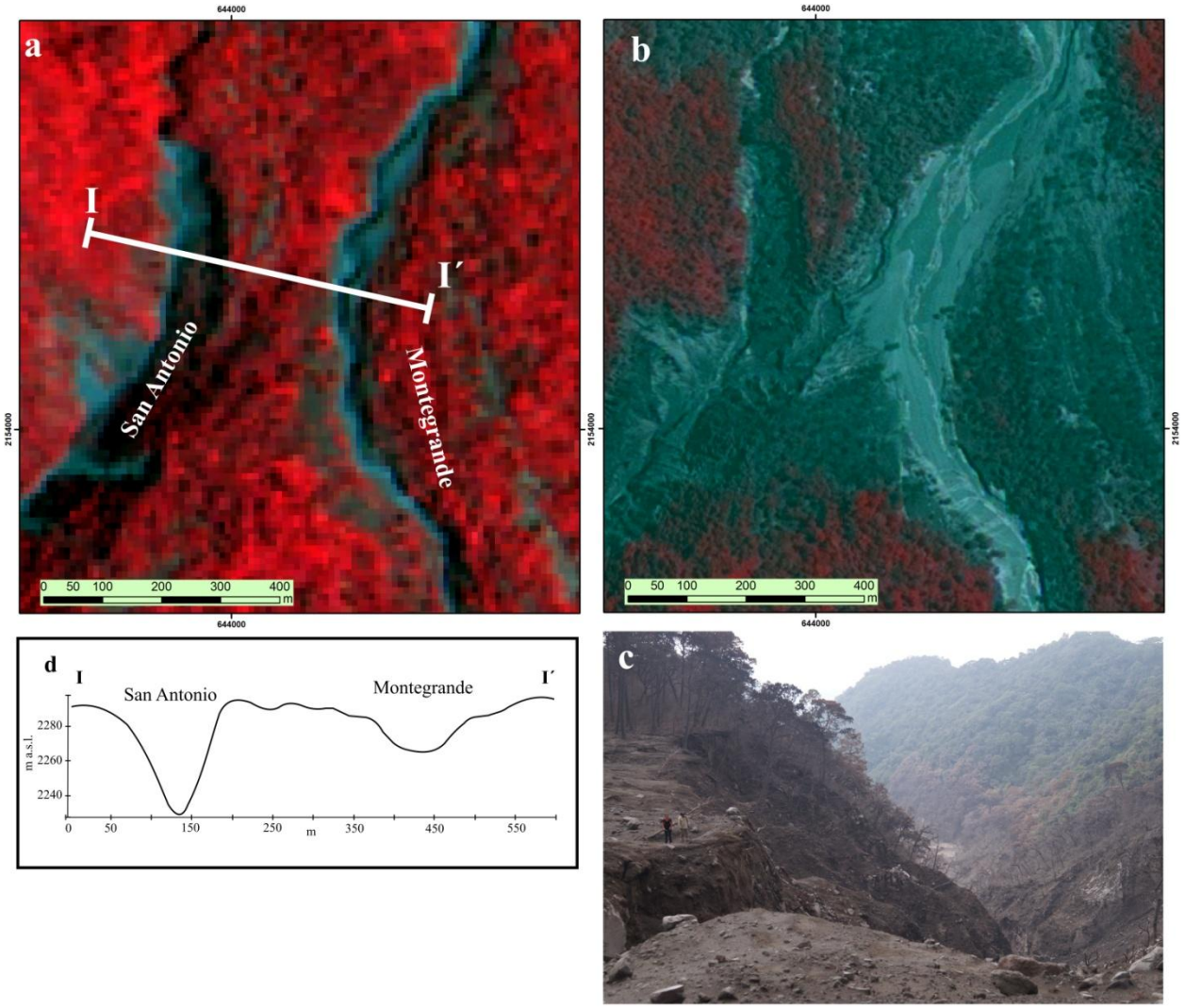

Figure 07

Figure 8

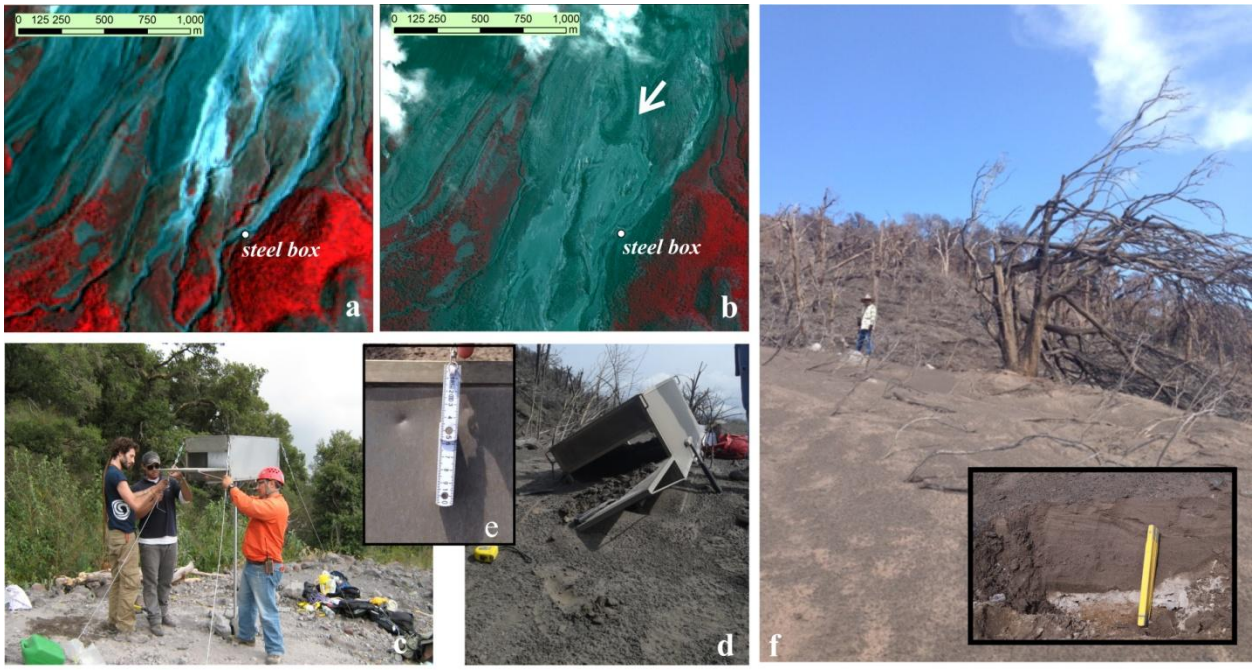

Figure 9

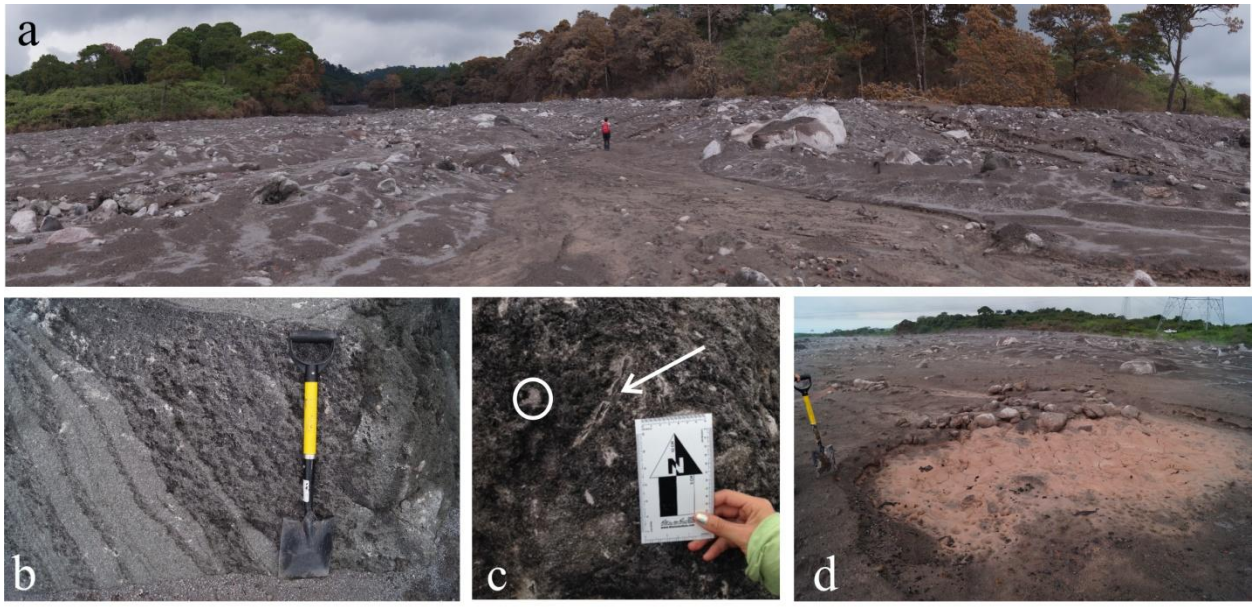

Figure 10

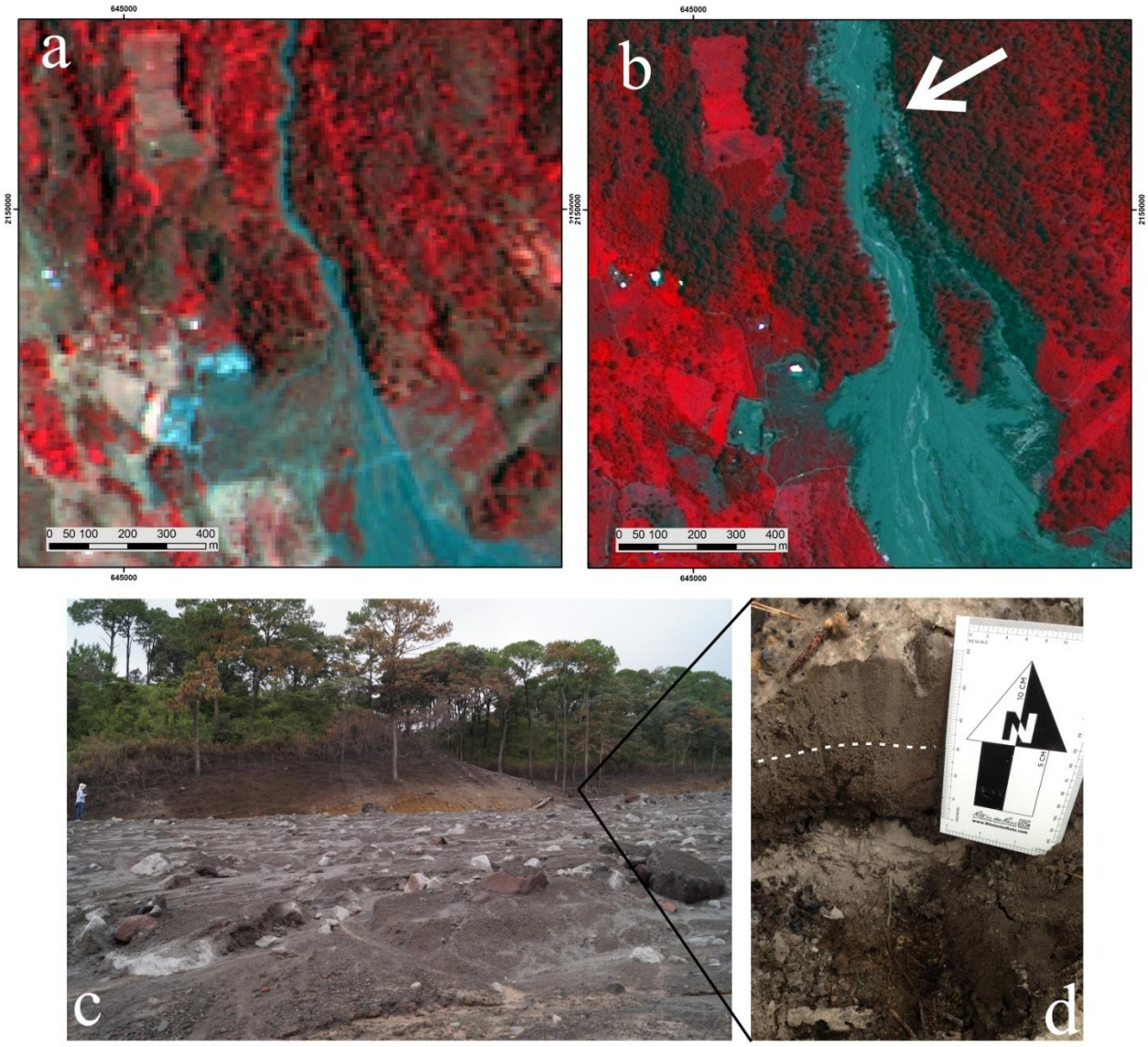

Figure 11

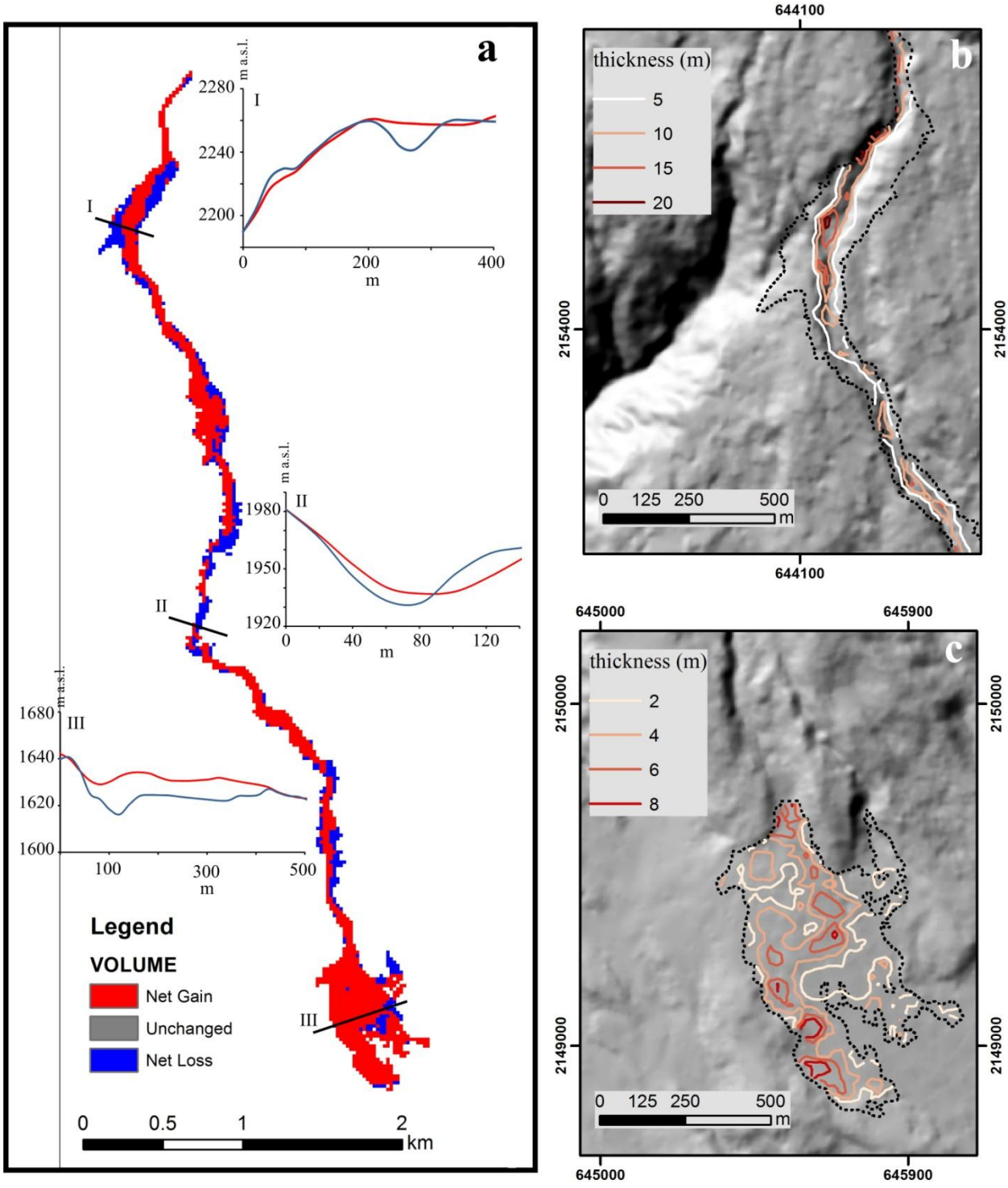

Figure 12

Highlights

The July 10-11, 2015 explosive eruption at Volcán de Colima originated the longest and hottest pyroclastic density currents recorded during the past 30 years.

The summit dome was destroyed and a new crater excavated and breached to the south.

An average volume of 4.5 X 10^6 m^3 was estimated for the deposits emplaced along the Montegrande ravine, with a H/L of 0.2

The juvenile components consist of dense and vesicular dark-gray lava blocks, with plagioclase + clinopyroxene + orthopyroxene + FeTi-oxides ± olivine and resorbed hornblende.